

Article

Neogene Alkali Basalts from Central Slovakia (Ostrá Lúka Lava Complex); Mineralogy and Geochemistry

Ján Spišiak ^{1,*}, Roberta Prokešová ², Juraj Butek ¹ and Viera Šimonová ¹

¹ Department of Geography and Geology, Faculty of Natural Sciences, Matej Bel University, Tajovského 40, SK-97401 Banská Bystrica, Slovakia; juraj.butek@umb.sk (J.B.); viera.simonova@umb.sk (V.Š.)

² Department of Physical Geography, Geomorphology and Natural Hazards, Institute of Geography, Slovak Academy of Sciences, Štefánikova 49, SK-81473 Bratislava, Slovakia; roberta.prokesova@savba.sk

* Correspondence: jan.spišiak@umb.sk

Abstract: Ostrá Lúka basalts are a product of the final phase of Neogene volcanism in Central Slovakia. Their major and trace elements composition is alkaline, a feature confirmed by light rare earth elements (LREE) relative enrichment and some incompatible trace elements ratios. The basalts contain rare surrounded gabbro cumulates. Their peculiarity is a strong zonation of olivines and clinopyroxene. The significant zonation probably indicates a short stop of the melt at shallow depth. The Sr, Nd and Pb isotope compositions indicate an origin from a moderately depleted mantle source. The mineral and chemical composition of the basalts is similar to the Pannonian basin alkali basalts and the Western and Central Europe alkali basalts.

Keywords: mineralogy; geochemistry; alkali basalt; Ostrá Lúka lava complex; Central Slovakia; Western Carpathians



Citation: Spišiak, J.; Prokešová, R.; Butek, J.; Šimonová, V. Neogene Alkali Basalts from Central Slovakia (Ostrá Lúka Lava Complex); Mineralogy and Geochemistry. *Minerals* **2022**, *12*, 195. <https://doi.org/10.3390/min12020195>

Academic Editors: Alexey V. Ivanov and Massimo D'Antonio

Received: 26 November 2021

Accepted: 29 January 2022

Published: 2 February 2022

Publisher's Note: MDPI stays neutral with regard to jurisdictional claims in published maps and institutional affiliations.



Copyright: © 2022 by the authors. Licensee MDPI, Basel, Switzerland. This article is an open access article distributed under the terms and conditions of the Creative Commons Attribution (CC BY) license (<https://creativecommons.org/licenses/by/4.0/>).

1. Introduction

All Neogene alkali basalts in the Western Carpathian part of the Carpathian-Panonian Region (CPR) have a similar chemical and mineral composition. The composition of the main rock-forming minerals of alkali basalts of the Carpathian region (olivines, clinopyroxenes) has been extensively studied, focusing on geochemistry and isotopic composition ([1–9] and others). In contrast, detailed mineral as well as chemical composition of the basalts of central Slovakia has been studied only marginally (e.g., [5,7,10,11], and others). Volcanological and geochronological studies have been performed in much more detail [12–17].

This study focuses on the mineralogy and geochemistry of basalts from the Ostrá Lúka lava complex (Central Slovakia). Our findings can be generalized for the area of the Western Carpathians and/or eventually for the whole Carpathian-Panonian Region (CPR).

2. Geological Settings

Alkali basalt (AB) volcanic activity represents the youngest phase of Cenozoic volcanism of the CPR (Figure 1a, [18]). Products of alkali basalt volcanism in this region are concentrated in four main volcanic fields and numerous scattered necks, lava flows and cinder cones [19]. In Slovakia, the products of volcanism are present in two volcanic areas, the South Slovakia Volcanic Field and the Central Slovakia Neogene Volcanic Field (CSNVF, Figure 1a). In both areas, the basaltic volcanic activity occurred discontinuously between 8.0 and 0.1(?) Ma [20] following the paroxysmal Middle Miocene (17–11 Ma) calc-alkaline volcanic phases [21].

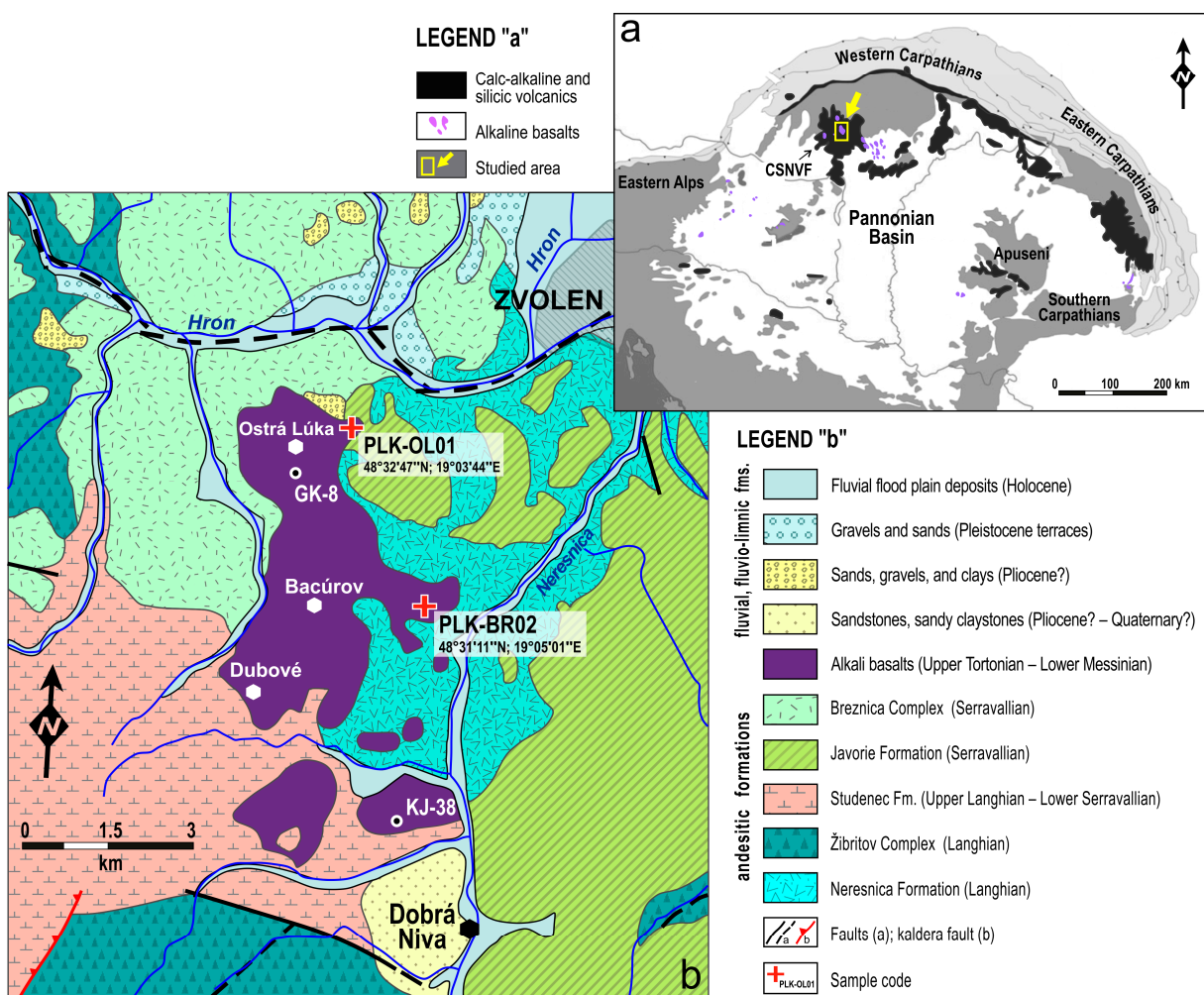


Figure 1. (a) Location of the CSNVF and Ostra Luka (OL) lava complex in the Carpathian-Pannonian Region; (b) Geological map of the OL lava complex and the surrounding area [22,23].

Volcanism in the CSNVF was initiated by back-arc extension related to subduction rollback and a contemporaneous uprise of the asthenospheric mantle [24]. Miocene crustal thinning and horst-and-graben tectonics were accompanied by long-lasting volcanism, climaxing during the Langhian and Serravallian. At that time, predominantly andesitic stratovolcanoes were formed in a mostly terrestrial environment [13,25–27]. For the largest CSNVF stratovolcano, Štiavnica Volcano, the time span and main phases of volcanic activity have been redefined by Chernyshev et al. [22] based on K-Ar and Rb-Sr data. Four stages of andesitic volcanism, followed by a fifth rhyolite stage, occurred between the Late Langhian (ca. 15.0 Ma) and Early Tortonian (11.4 Ma). Later on, episodic effusions (not defined as separate volcanic stages) of high alumina basalts and alkali basalts occurred between ca. 8.0 and 0.1(?) Ma.

Ostrá Lúka basalts (OL basalts) are the largest AB complex of the CSNVF, covering an area of about 22 km². The OL volcano was likely active for a long period of more than one million years in the Upper Miocene (6.6–7.8 Ma), as suggested by previous [26] and new Ar/Ar (whole-rock) dating of basalt (unpublished raw data). Thus, the OL basalts likely represent only an erosion remnant of an initially more extensive volcanic complex formed by several lava flows. At present, the lava complex forms a volcanic plateau situated roughly between Zvolen and Dobrá Niva (Figure 1b).

Basalt plateau thickness up to 40–50 m was established by boreholes GK-8 and KJ-38 [27] and geoelectric profiling. Due to flat topography and relatively smooth relief with slightly incised streams, the outcrops of basalt flows are relatively scarce. Nevertheless, the

basalts are occasionally exposed along local terrain edges near Ostrá Luka and Bacurov, where samples of relatively fresh (unweathered) rock were collected (Figure 1b).

3. Analytical Methods

Eight basalt samples were collected from Ostrá Lúka lava complex. All samples had similar textures, structures and mineral composition. Two samples were chosen for a detailed study. Silicate minerals were analysed using electron microprobe JEOL JXA 8530FE at the Earth Sciences Institute in Banská Bystrica under the following conditions: accelerating voltage 15 kV, probe current 20 nA, beam diameter 3–8 µm, ZAF correction, counting time 10 s on peak, 5 s on background. The used standards, X-ray lines and D.L. (in ppm) were as follows: Ca ($K\alpha$, 25)—diopside, K ($K\alpha$, 44)—orthoclase, P ($K\alpha$, 41)—apatite, F ($K\alpha$, 167)—fluorite, Na ($K\alpha$, 43)—albite, Mg ($K\alpha$, 41)—diopside, Al ($K\alpha$, 42)—albite, Si ($K\alpha$, 63)—quartz, Ba ($L\alpha$, 72)—barite, Fe ($K\alpha$, 52)—hematite, Cr ($K\alpha$, 113)— Cr_2O_3 , Mn ($K\alpha$, 59)—rhodonite, Ti ($K\alpha$, 130)—rutile, Cl ($K\alpha$, 12)—tugtupite, Sr ($L\alpha$, 71)—celestite.

Whole rock chemical compositions were determined at the ACME Analytical Laboratories (Vancouver, Canada). Total abundances of major element oxides were determined by inductively coupled plasma emission spectrometry (ICP-ES) following lithium metaborate–tetraborate fusion and dilute nitric acid treatment. Loss on ignition (LOI) was calculated from the difference in weight after ignition to 1000 °C. For the total carbon (TOT/C) and sulphur analysis (TOT/S) by LECO analysis, the samples were heated in an induction furnace to >1650 °C, which caused the volatilization of all C and S bearing phases. Vapours were carried through an infrared spectrometric cell wherein the concentrations of C and S were determined by the absorption of specific wavelengths in the infrared spectra ($\text{ORG/C} = \text{TOT/C}$ minus graphite C and carbonate). Concentrations of trace elements and rare earth elements were determined by ICP mass spectrometry (ICP-MS). Further details are accessible on the web page of the ACME Analytical Laboratories (<http://acmelab.com/>).

The samples were analyzed for Pb and Sr isotopes using a VG Sector 54 IT thermal ionization mass spectrometer (TIMS) at the Department of Geosciences and Natural Resource Management, University of Copenhagen, Denmark. The powdered samples were dissolved by standard procedures using concentrated HNO_3 , HCl and HF within Savillex™ beakers on a hotplate at 130 °C for 3 days. A $^{150}\text{Nd}/^{147}\text{Sm}$ spike was added beforehand. The isotopic ratios of Sm, Nd, Pb and Sr, and of Sm and Nd isotopic dilution concentrations were determined from separately dissolved powder aliquots using a VG Sector 54 IT Thermal Ionization Mass Spectrometer (TIMS) at IGN. Samples were separated over chromatographic columns charged with 12 mL AG50W-X 8 (100–200 mesh) cation resin, where Sr and REE fractions were collected. REE fractions were further separated over smaller chromatographic columns containing Eichrom's™ LN resin SPS (Part#LN-B25-S, Lisle, Illinois). Sr cuts were purified applying a standardized 3M $\text{HNO}_3\text{-H}_2\text{O}$ elution recipe on self-made disposable mini-extraction columns, which consisted of 1mL pipettetips in which we fitted a frit filter to retain 0.2 mL intensively pre-cleaned mesh 50–100 SrSpec™ (Eichrome Inc.) resin. The elution recipe essentially followed that of Horwitz et al. [28], scaled to our needs. Sr was eluted/stripped by pure deionized water and then the eluate was dried on a hotplate. Samarium isotopes were measured in a static multi-collection mode, whereas Nd isotopes were collected in a multi-dynamic routine, both on a triple Ta-Re-Ta filament setting. The measured Nd isotope ratios were normalized to $^{146}\text{Nd}/^{144}\text{Nd} = 0.7219$. The mean value of $^{143}\text{Nd}/^{144}\text{Nd}$ ratios for our JNd standard runs during the period the samples were analyzed amounted to 0.512105 ± 5 (2σ ; $n = 8$). Precision for $^{147}\text{Sm}/^{144}\text{Nd}$ ratios is better than 2% (2σ). Chemical separation of Pb from the whole rock samples was performed over conventional glass stem and subsequently miniature glass stem anion exchange columns containing, respectively, 1 mL and 200 L of 100–200 mesh Bio-Rad AG 1 × 8 resin. Pb was analyzed in a static multi-collection mode where fractionation was controlled by repeated analysis of the NBS 981 standard (using values of Todt et al. [29]). The average fractionation amounted to $0.105 \pm 0.008\%$ (2σ ,

$n = 5$) per atomic mass unit. Total procedural blanks remained below <200 pg Pb which, compared to >100 ng Pb loads, insignificantly affected the measured Pb isotopic ratios of the samples.

4. Mineralogy

The texture, structure and mineral composition of the basalt samples from the studied lava flows are similar. They are dark gray, non- or low-vesicular and the matrix is microlithic-porphyritic with plagioclase, olivine and pyroxene larger crystals. Common alkaline minerals as nepheline and leucite are occasionally present. Locally, the basalts contain oval coarser-grained gabbro cumulates (up to 5 mm in size) with relatively sharp boundaries (Figure 2a,b). Clinopyroxenes of similar composition in basalts and coarser-grained cumulates suggests that the latter come from co-genetic gabbro cumulates.

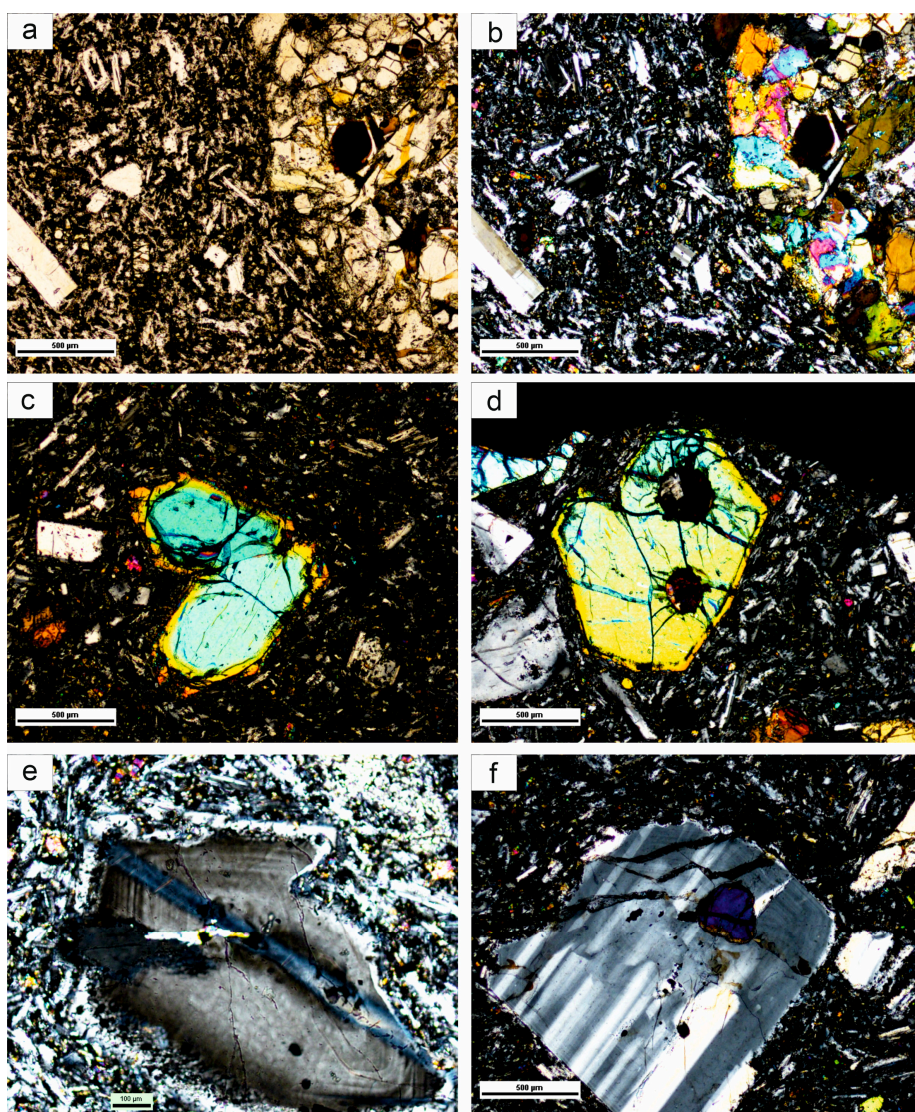


Figure 2. Photomicrograph: (a) contact of basalts with cumulates, parallel polaroids, (b) the same, crossed polaroids, (c,d) zonal olivines, crossed polaroids, (e,f) plagioclase phenocrysts, crossed polaroids.

Olivine is the dominant phenocryst phase but it is also present in the fine-grained matrix. It is only weakly altered. The larger crystals are subhedral, whereas the smaller ones are euhedral. Olivine is only present at the edge of gabbro cumulates. Olivine is characteristically zoned (Figure 2c,d and Figure 3c). However, it is not a classical oscillatory

zoning, but two relatively separate phases. The central parts (cores) of the olivines have a high content of the forsterite component (Fo85), whereas the rims have a significantly lower content of the forsterite component (Fo62, Table 1, Figure 5). This composition reflects a re-equilibration (mainly pressure change) during the formation of the different olivine phases with olivines, with Fo85 probably in equilibrium with a more primitive melt.

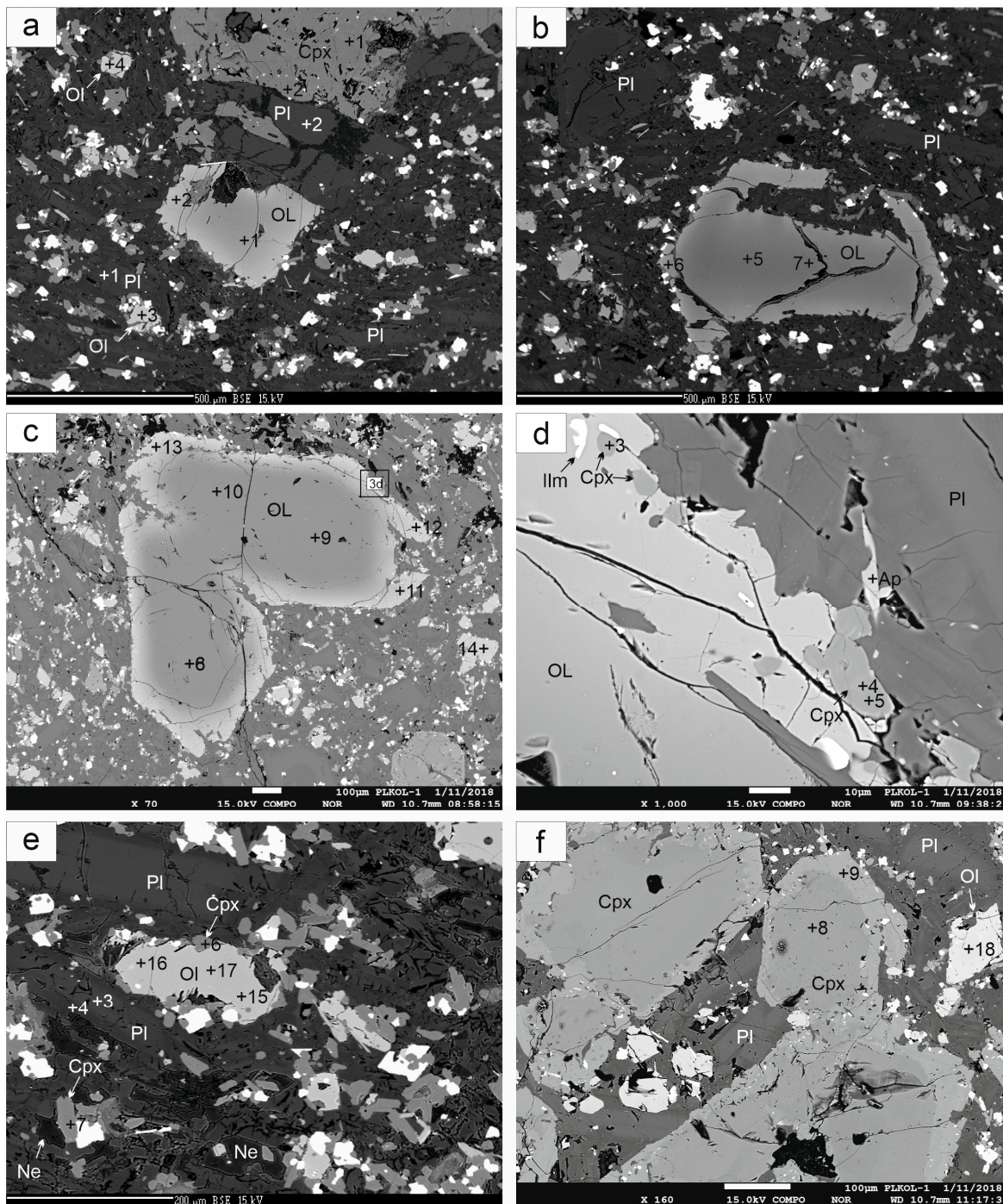


Figure 3. (a,b) Back scattered electron (BSE) images of olivines, clinopyroxenes and plagioclases; (c) BSE image of zonedg olivines (the same as Figure 2c); (d) detail of rims of olivines; (e) BSE image of olivines, clinopyroxenes and plagioclases, (f) BSE image of zonal Cpx; (Pl—plagioclase, Ol—olivine, Cpx—clinopyroxene, Ilm—ilmenite, Ne—nepheline); the numbers in figures correspond to those in Tables 1–3.

Table 1. Chemical composition of olivines.

Sample		PLK BR-2					PLKOL-1					PLK BR-2					PLKOL-1							
Ana No		1	2	3	4	5	6	7	8	9	10	11	12	13	14	15	16	17	18	19	20	21	22	
Figures	3a	3a	3a	3a	3b	3b	3b	3c	3c	3c	3c	3c	3c	3c	3e	3e	3e	3f	4c	4d	4e	4e	4e	
SiO ²	37.57	36.24	35.92	35.74	38.35	36.69	37.88	39.60	40.25	39.78	36.88	36.98	36.80	36.87	35.82	35.65	36.13	36.06	37.55	36.35	37.52	37.50		
TiO ²	0.02	0.04	0.06	0.04	0.02	0.04	0.03	0.09	0.03	0.11	0.07	0.16	0.09	0.02	0.12	0.06	0.04	0.01	0.03	0.10	0.00	0.02		
Al ² O ³	0.00	0.02	0.05	0.03	0.03	0.01	0.07	0.09	0.05	0.03	0.01	0.01	0.03	0.03	0.00	0.01	0.00	0.03	0.15	0.04	0.02	0.02		
Cr ² O ³	0.02	0.00	0.00	0.00	0.00	0.01	0.00	0.00	0.00	0.00	0.00	0.00	0.00	0.00	0.02	0.00	0.00	0.01	0.09	0.00	0.02	0.02		
FeO [*]	26.53	32.77	35.59	34.70	22.90	31.43	23.90	14.50	14.27	14.26	31.76	31.91	31.73	32.72	36.31	35.41	34.79	33.09	34.49	34.55	28.50	28.05		
MnO	0.49	0.70	0.87	0.85	0.38	0.67	0.46	0.14	0.12	0.19	0.49	0.53	0.46	0.62	0.85	0.81	0.86	0.60	0.32	0.73	0.39	0.37		
CaO	0.22	0.35	0.37	0.36	0.21	0.35	0.21	0.22	0.20	0.20	0.32	0.31	0.34	0.30	0.41	0.38	0.37	0.34	0.51	0.66	0.34	0.27		
MgO	35.38	30.17	27.15	27.61	37.93	30.89	37.23	44.50	44.98	44.41	30.34	29.99	30.45	29.18	26.59	27.19	28.49	28.58	26.23	27.14	32.83	33.37		
NiO	0.00	0.00	0.00	0.02	0.07	0.00	0.06	0.00	0.00	0.00	0.00	0.00	0.00	0.00	0.00	0.00	0.00	0.00	0.00	0.00	0.00	0.00		
Na ₂ O	0.00	0.03	0.05	0.00	0.06	0.02	0.00	0.03	0.00	0.03	0.02	0.00	0.03	0.00	0.01	0.08	0.06	0.04	0.00	0.07	0.00	0.00		
K ² O	0.00	0.00	0.00	0.00	0.00	0.01	0.00	0.00	0.00	0.00	0.00	0.00	0.00	0.00	0.00	0.01	0.00	0.00	0.00	0.00	0.00	0.00		
Total	100.22	100.32	100.06	99.35	99.94	100.11	99.84	99.17	99.90	99.00	99.89	99.89	99.94	99.75	100.13	99.61	100.73	98.75	99.38	99.63	99.60	99.60		
Formula based on 4 oxygens																								
Si	0.996	0.992	1.003	1.001	1.003	1.000	0.996	1.002	1.009	1.008	1.010	1.015	1.007	1.018	1.004	1.000	0.996	1.009	1.057	1.018	1.014	1.010		
Ti	0.000	0.001	0.001	0.001	0.000	0.001	0.001	0.002	0.001	0.002	0.002	0.003	0.002	0.000	0.003	0.001	0.001	0.000	0.001	0.002	0.000	0.000		
Al	0.000	0.001	0.002	0.001	0.001	0.000	0.002	0.003	0.001	0.001	0.000	0.000	0.001	0.001	0.000	0.000	0.000	0.001	0.005	0.001	0.001	0.001		
Cr	0.000	0.000	0.000	0.000	0.000	0.000	0.000	0.000	0.000	0.000	0.000	0.000	0.000	0.000	0.001	0.000	0.000	0.000	0.002	0.000	0.000	0.000		
Fe ³⁺	0.007	0.015	0.000	0.000	0.000	0.000	0.005	0.000	0.000	0.000	0.000	0.000	0.000	0.000	0.000	0.000	0.000	0.007	0.000	0.000	0.000	0.000		
Fe ²⁺	0.581	0.735	0.831	0.813	0.501	0.717	0.521	0.307	0.299	0.302	0.728	0.733	0.726	0.756	0.851	0.831	0.795	0.774	0.812	0.809	0.644	0.632		
Mn	0.011	0.016	0.021	0.020	0.008	0.015	0.010	0.003	0.003	0.004	0.011	0.012	0.011	0.014	0.020	0.019	0.020	0.014	0.008	0.017	0.009	0.008		
Mg	1.398	1.231	1.131	1.153	1.480	1.256	1.460	1.678	1.682	1.678	1.239	1.227	1.243	1.201	1.110	1.137	1.171	1.192	1.100	1.133	1.322	1.340		
Ca	0.006	0.010	0.011	0.011	0.006	0.010	0.006	0.006	0.005	0.009	0.010	0.009	0.012	0.011	0.011	0.010	0.015	0.020	0.010	0.020	0.010	0.008		
End members (%)																								
Fo	69.789	61.321	56.712	57.738	74.164	62.842	72.930	84.163	84.556	84.340	62.353	61.941	62.456	60.662	55.701	56.903	58.439	59.881	56.859	57.245	66.620	67.408		
Fa	29.354	37.355	41.705	40.712	25.122	35.866	26.263	15.387	15.047	15.190	36.608	36.976	36.506	38.159	42.681	41.567	40.023	38.903	41.948	40.881	32.443	31.782		

FeO * total Fe as FeO.

Table 2. Chemical composition of clinopyroxenes.

Sample	PLKBR-2			PLKOL-1			PLKBR-2			PLKOL-1			Gabbro Cumulates			
Anal. No.	1	2	3	4	5	6	7	8	9	10	11	12	13	14	15	
Figures	3a	3a	3d	3d	3d	3e	3e	3f	3f	4c	4c	4d	4f	4f	4f	
SiO ₂	47.97	50.32	49.61	48.78	51.67	50.40	50.89	49.43	48.81	49.44	49.63	51.68	51.91	48.83	49.84	
TiO ₂	2.19	1.69	2.25	2.76	1.59	1.75	1.60	1.61	2.02	1.53	1.55	1.36	1.23	1.49	1.22	
Al ₂ O ₃	6.84	3.45	3.24	4.28	2.16	2.47	2.21	6.60	5.28	6.21	6.99	2.42	1.94	7.61	6.83	
Cr ₂ O ₃	0.06	0.06	0.02	0.00	0.00	0.00	0.01	0.25	0.02	0.10	0.08	0.00	0.07	0.20	0.92	
FeO *	7.98	7.75	10.25	9.50	8.65	8.58	8.25	6.01	7.86	7.23	5.86	8.75	8.29	5.52	4.63	
MnO	0.14	0.20	0.25	0.29	0.22	0.21	0.23	0.18	0.21	0.19	0.08	0.20	0.21	0.21	0.07	
CaO	21.02	21.74	20.68	21.30	21.32	21.87	21.89	20.55	21.76	20.36	20.56	21.34	21.40	20.71	20.48	
MgO	13.14	14.29	13.18	12.57	13.94	14.16	14.30	14.55	13.44	14.32	14.67	13.69	14.16	14.29	14.77	
Na ₂ O	0.63	0.47	0.37	0.49	0.34	0.45	0.51	0.39	0.35	0.46	0.48	0.42	0.40	0.52	0.50	
K ₂ O	0.01	0.02	0.00	0.00	0.00	0.03	0.02	0.00	0.00	0.00	0.00	0.00	0.00	0.00	0.00	
Total	99.98	99.99	99.84	99.98	99.89	99.92	99.91	99.57	99.75	99.85	99.90	99.86	99.61	99.37	99.27	
Formula based on 6 oxygens																
Si	1.779	1.866	1.864	1.830	1.930	1.877	1.893	1.826	1.819	1.827	1.823	1.930	1.939	1.802	1.839	
Ti	0.061	0.047	0.064	0.078	0.045	0.049	0.045	0.045	0.057	0.043	0.043	0.038	0.035	0.041	0.034	
Al	0.299	0.151	0.143	0.189	0.095	0.109	0.097	0.287	0.232	0.271	0.303	0.106	0.085	0.331	0.297	
Cr	0.002	0.002	0.000	0.000	0.000	0.000	0.000	0.007	0.001	0.003	0.002	0.000	0.002	0.006	0.027	
Fe ³⁺	0.064	0.055	0.027	0.030	0.000	0.072	0.065	0.000	0.043	0.021	0.000	0.000	0.000	0.013	0.000	
Fe ²⁺	0.183	0.185	0.295	0.268	0.270	0.196	0.192	0.186	0.202	0.203	0.180	0.273	0.259	0.158	0.143	
Mn	0.004	0.006	0.008	0.009	0.007	0.007	0.007	0.006	0.007	0.006	0.002	0.006	0.007	0.007	0.002	
Mg	0.726	0.790	0.738	0.703	0.776	0.786	0.793	0.802	0.747	0.789	0.803	0.762	0.788	0.787	0.813	
Ca	0.835	0.864	0.833	0.856	0.853	0.873	0.872	0.814	0.869	0.806	0.809	0.854	0.856	0.819	0.810	
Na	0.045	0.034	0.027	0.036	0.025	0.032	0.037	0.028	0.025	0.033	0.034	0.030	0.029	0.037	0.036	
End members (%)																
Wo	46.174	45.597	43.975	46.104	44.913	45.308	45.390	45.178	46.697	44.335	45.141	45.201	44.985	46.109	45.869	
En	40.142	41.709	39.007	37.849	40.867	40.813	41.254	44.504	40.132	43.370	44.822	40.330	41.409	44.289	46.032	
Fs	13.684	12.694	17.018	16.047	14.220	13.878	13.356	10.318	13.171	12.294	10.037	14.469	13.606	9.602	8.099	
Mg#	0.798	0.81	0.714	0.724	0.742	0.801	0.805	0.812	0.787	0.796	0.817	0.736	0.753	0.833	0.85	

FeO * total Fe as FeO.

The composition of the cores of olivine phenocrysts corresponds to that of olivine from alkali basalts ([10,30,31] and others). The rims have relatively sharp boundaries with the cores and display lower Mg contents (Fo65-60) that suggest a re-equilibration during magma ascent toward the surface (with a likely short-term suspension of the ascent). Such a composition is relatively rare and is probably due to the magmatic alteration of olivine that affects the mineral phases prior to eruption, in the magmatic chamber. Changes in olivine composition also correspond to changes in clinopyroxenes. Clinopyroxene rims have higher Ti/Al ratios compared to the cores, which indicates their formation at lower

pressures. Except for the significant change in Mg and Fe contents in olivines during “high temperature corrosion”, only minor changes are observed for the other elements. The Mn and Ca contents decrease with the increase Mg # number in olivine (Figure 4). The Cr and Ni contents in the analysed olivines are very low. High temperature corrosions of olivine have also been studied in detail in recent lavas [32,33]. From the Carpathian region, high temperature corrosion of olivine phenocrysts in basalts from Banat has been described [34]. Groundmass olivines have a composition similar to the rims of olivine phenocrysts.

Table 3. Chemical composition of plagioclases.

Sample	PLKBR-2										PLKOL-1				Gabbro Cumulates	
	Anal N.	1	2	3	4	5	6	7	8	9	10	11	12	13	14	15
Figures	3a	3a	3e	3e	4b	4b	4b	4c	4c	4c	4c	4d	4d	4f	4f	
SiO ₂	57.37	53.93	54.20	65.44	55.86	52.50	57.83	53.29	56.07	52.00	52.64	63.16	62.54	58.68	51.42	
TiO ₂	0.00	0.00	0.00	0.00	0.00	0.00	0.00	0.22	0.06	0.00	0.22	0.09	0.21	0.19	0.17	
Al ₂ O ₃	26.07	28.66	28.12	19.70	27.34	29.59	25.64	29.42	27.00	30.07	28.93	21.28	21.65	24.65	29.21	
FeO *	0.63	0.38	0.75	0.33	0.37	0.37	0.84	0.18	0.29	0.30	0.66	0.25	0.30	0.48	0.44	
MnO	0.00	0.00	0.00	0.00	0.00	0.00	0.00	0.07	0.00	0.02	0.04	0.02	0.00	0.08	0.00	
CaO	9.18	11.96	11.70	1.60	10.59	12.89	8.15	12.02	9.08	12.79	11.90	2.81	3.35	7.07	12.48	
MgO	0.00	0.02	0.01	0.00	0.03	0.02	0.06	0.03	0.02	0.05	0.02	0.01	0.02	0.02	0.06	
BaO	0.00	0.00	0.00	0.00	0.00	0.00	0.00	0.01	0.06	0.00	0.02	0.04	0.19	0.07	0.00	
SrO	0.11	0.14	0.17	0.05	0.17	0.16	0.07	0.09	0.17	0.18	0.22	0.13	0.11	0.17	0.22	
Na ₂ O	5.59	4.26	4.43	6.37	4.89	3.89	6.24	4.40	5.91	4.06	4.42	7.24	7.30	6.71	3.83	
K ₂ O	0.55	0.33	0.31	5.91	0.45	0.26	0.73	0.29	0.59	0.22	0.27	4.28	3.50	0.89	0.30	
	99.49	99.67	99.68	99.40	99.70	99.56	99.56	100.01	99.25	99.69	99.33	99.30	99.17	99.01	98.13	

Formula based on 8 oxygens															
Si	2.608	2.462	2.475	2.960	2.543	2.399	2.614	2.419	2.545	2.371	2.411	2.844	2.823	2.664	2.389
Ti	0.000	0.000	0.000	0.000	0.000	0.000	0.000	0.007	0.002	0.000	0.008	0.003	0.007	0.006	0.006
Al	1.397	1.542	1.514	1.050	1.467	1.594	1.366	1.574	1.444	1.616	1.561	1.129	1.151	1.319	1,600
Cr	0.000	0.000	0.000	0.000	0.000	0.000	0.000	0.000	0.000	0.000	0.000	0.000	0.000	0.000	0.000
Fe ³⁺	0.000	0.000	0.000	0.000	0.000	0.000	0.000	0.000	0.000	0.000	0.000	0.000	0.000	0.000	0.000
Fe ²⁺	0.024	0.014	0.029	0.012	0.014	0.014	0.032	0.007	0.011	0.011	0.025	0.009	0.011	0.018	0.017
Mn	0.000	0.000	0.000	0.000	0.000	0.000	0.000	0.003	0.000	0.001	0.001	0.001	0.000	0.003	0.000
Mg	0.000	0.001	0.000	0.000	0.002	0.002	0.004	0.002	0.001	0.004	0.001	0.000	0.001	0.001	0.004
Ca	0.447	0.585	0.572	0.078	0.517	0.631	0.395	0.585	0.442	0.625	0.584	0.136	0.162	0.344	0.621
Ba	0.000	0.000	0.000	0.000	0.000	0.000	0.000	0.000	0.001	0.000	0.000	0.001	0.003	0.001	0.000
Na	0.492	0.377	0.392	0.559	0.432	0.344	0.547	0.387	0.520	0.359	0.393	0.632	0.639	0.591	0.345
K	0.032	0.019	0.018	0.341	0.026	0.015	0.042	0.017	0.034	0.013	0.016	0.246	0.202	0.052	0.017

End members (%)															
An	46.049	59.624	58.260	7.930	53.027	63.712	40.115	59.140	44.325	62.693	58.859	13.387	16.167	34.866	63.136
Ab	50.689	38.406	39.916	57.195	44.300	34.753	55.584	39.190	52.229	36.038	39.575	62.371	63.729	59.890	35.086
Or	3.261	1.970	1.825	34.875	2.672	1.536	4.302	1.670	3.446	1.269	1.566	24.242	20.105	5.244	1.778

FeO * total Fe as FeO.

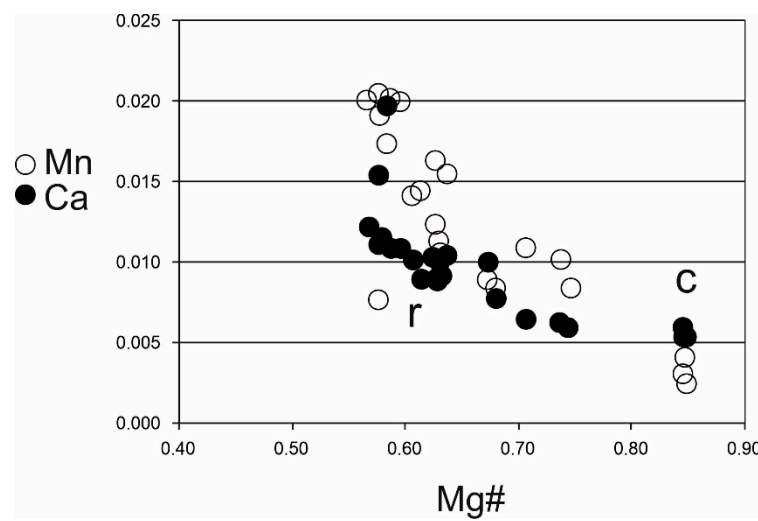


Figure 4. Plot of Ca and Mn vs. Mg—number in olivine from alkaline basalts (this study); c—core, r—rims.

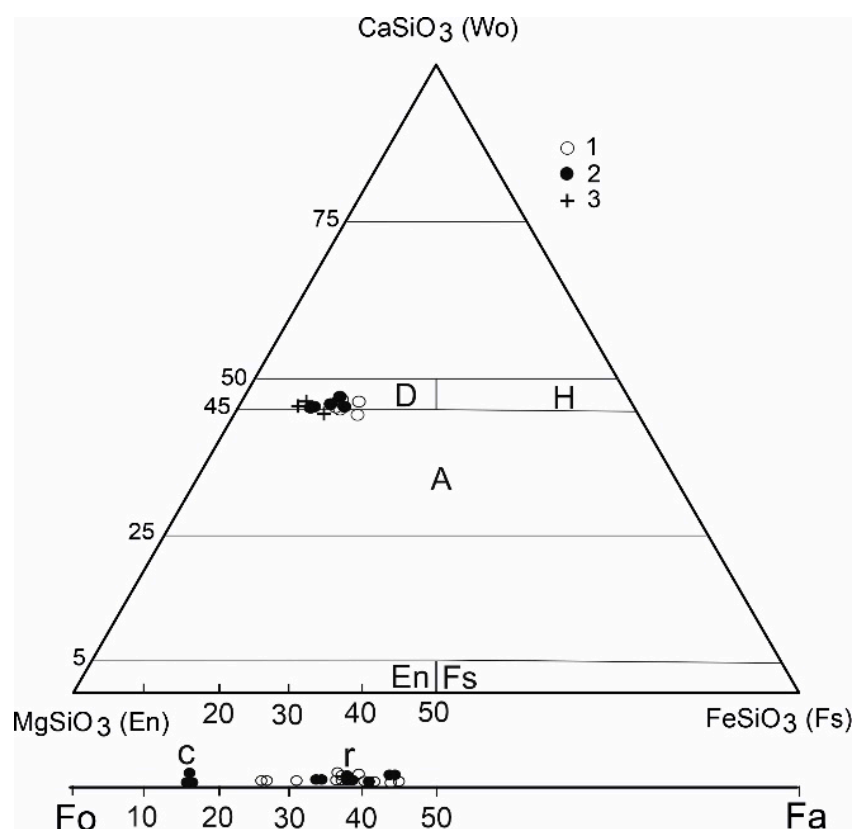


Figure 5. Classification diagram of clinopyroxenes [35], and olivines, D—diopside, H—hedenbergite, A—augite; c—core, r—rims, sample: 1—PLKBR-2, 2—PLKOL-1; 3—gabbro cumulates.

The clinopyroxene phenocrysts are usually zoned, either showing concentric and rarely sector zoning. The variation between core and rim compositions is not large (Table 2, Figure 3f) and follows the normal fractionation trend; the cores have higher Mg, Si and Cr and lower Fe, Ti, Ca and Al than the rims. But the Cr contents in Cpx in alkali basalts have relatively large variations [3,4]. We did not observe high Ti-augite Cpx phenocrysts that are common in alkali basalts [3,9]. However, the marginal parts of the phenocrysts poikilically enclose a large number of ilmenite grains (Figure 3f). It is probable that the rims of Cpx phenocrysts were originally formed by Ti-augite, which was changed by later processes. Based on a significant change in the Ti/Al ratio but also in the Al^{IV}/Al^{VI} ratio (Figure 6), we assume that basaltic magma stopped for a short time during ascent, then the composition of clinopyroxene rims (and olivine rims as well) changed by reaction with the melt. Decompression probably played a dominant role in the change of the Cpx and Ol composition. The composition of coarse-grained Cpx from gabbro cumulates is similar to the central parts of phenocrysts. Tiny Cpx are often lined with olivine phenocrysts (Figure 3d). The compositions of clinopyroxenes (based on the IMA nomenclature, [35]) are displayed in Figure 5. The majority of analyzed pyroxenes plot in the diopside field, but some plot in the augite field. The composition of clinopyroxene is similar to that of colorless phenocrysts of alkali basalts from western Pannonia Basin with a high Mg # 80–85 [9]. Variations in the Cpx composition are shown in Figure 6. The central parts of clinopyroxene correspond to the composition of porphyritic and megacrystic clinopyroxenes from alkali basalt of the western Pannonian Basin [8,9] but also to other Neogene alkali basalts [3]. The rims of clinopyroxenes have a different composition with a lower Mg # and Al contents.

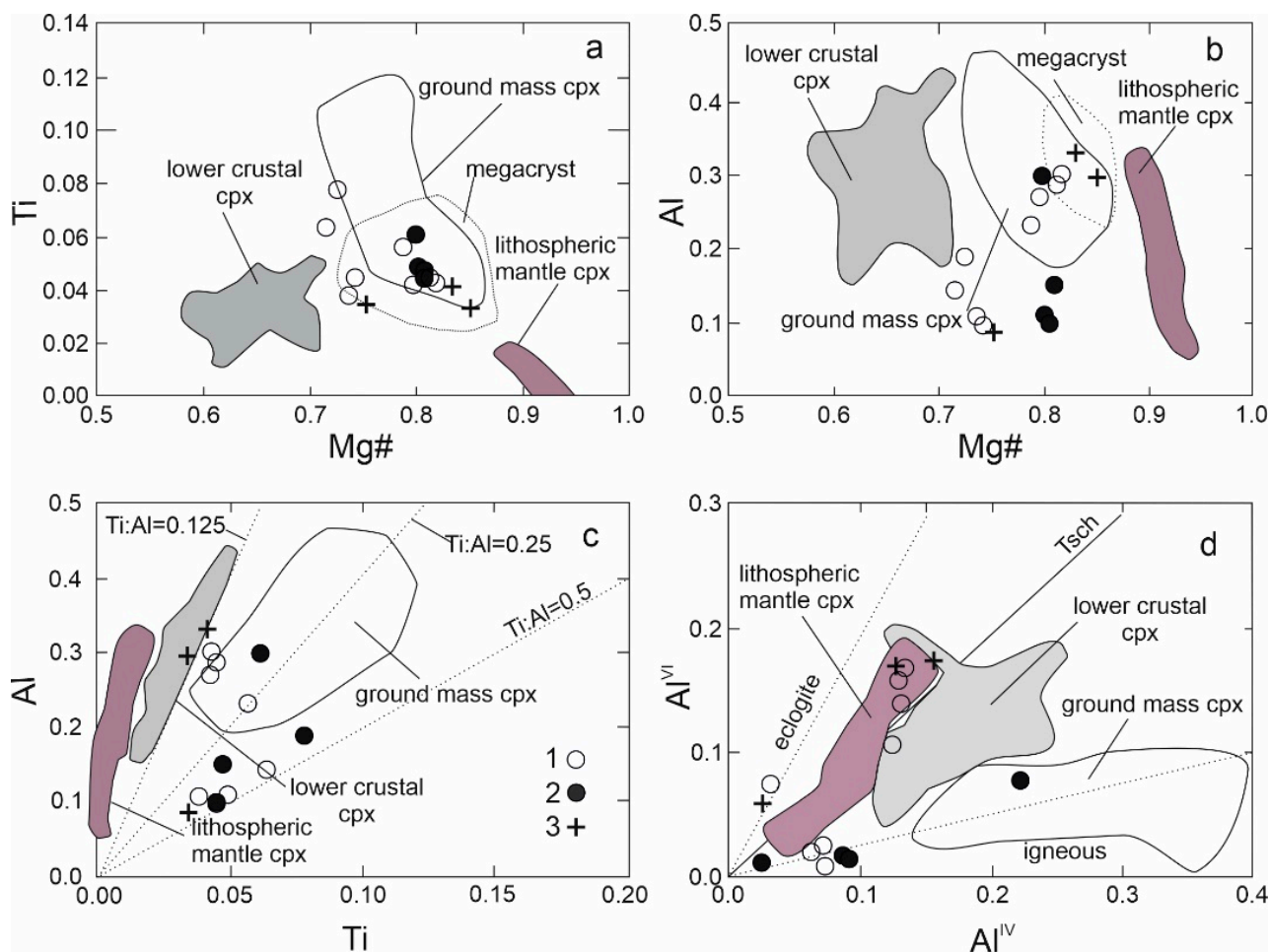
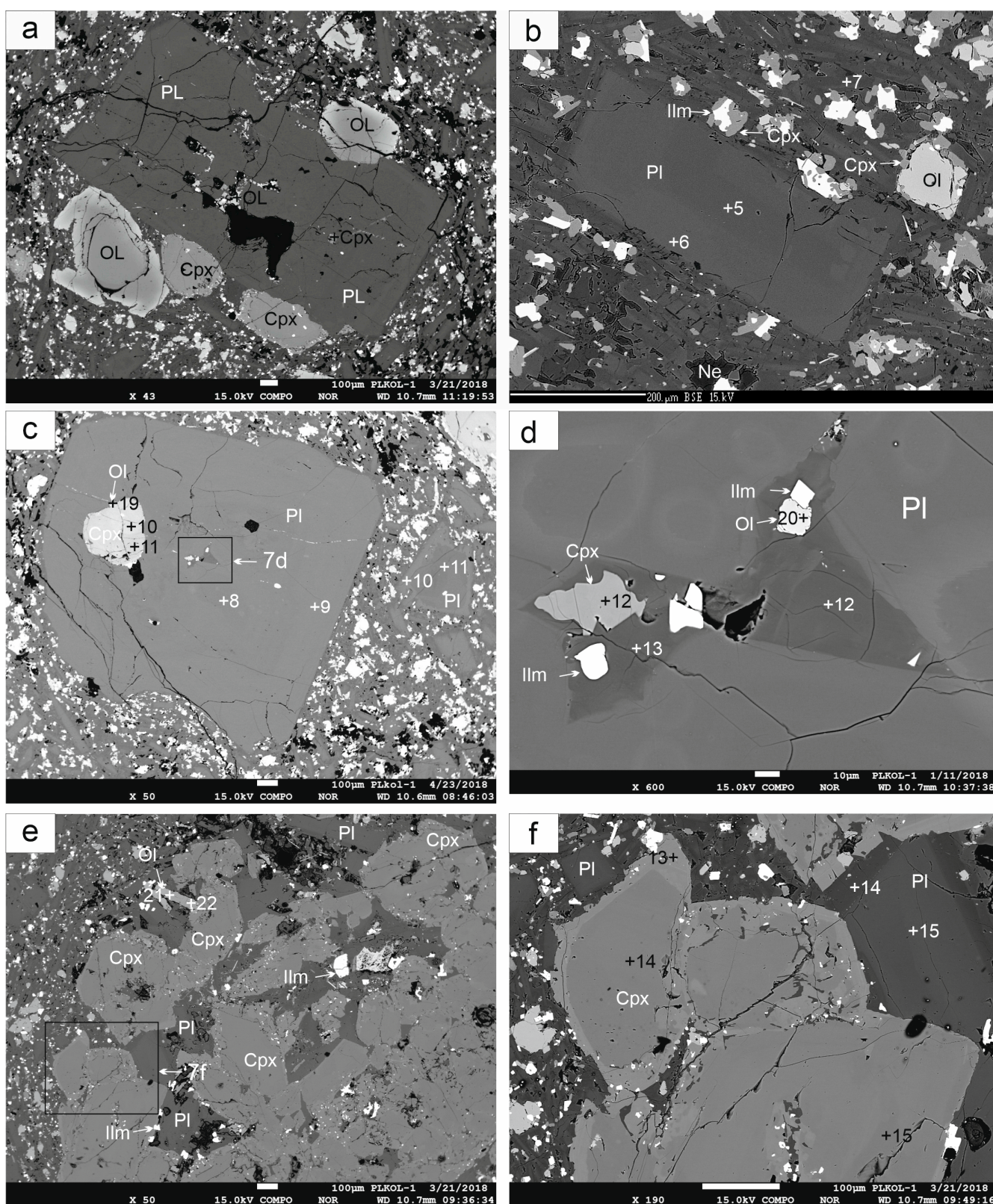


Figure 6. Variation of Mg# vs. Ti (a) Al (b) in clinopyroxene; (c,d) Plot of Ti vs. Al and Al^{IV} vs. Al^{VI} [36], symbols as in Fig 4. Field for pyroxene of alkaline basalts from the western Pannonian basin; according to Jankovic et al. [8].

The presence of orthopyroxene was rarely confirmed under the microscope and was not detected in the analyzed polished thin sections.

Plagioclase occurs as phenocrysts and in the matrix as well (Figure 2e,f). Plagioclase phenocrysts are zoned and often enclose olivine, clinopyroxene, and ilmenite grains (Figure 7a,c). Reverse zoning is manifested by an increase in anorthite content from the cores to the rims (from An53 to An62; Table 3). Plagioclase in the marginal parts of gabbro cumulates has a similar zonation (from An35 to An63, Figure 5f). Mihaliková and Šimová [10] also found this type of zoning in some localities of alkali basalts in Central and Southern Slovakia. The composition of plagioclase is plotted in Figure 8. Locally, tiny dark K-feldspar cumulates were found in the central parts of plagioclase phenocrysts (together with olivine, clinopyroxenes and ilmenite).

The alkali character of the studied basalts is confirmed by the absence of quartz and the presence of nepheline. Nepheline is relatively rare and forms tiny irregular grains. It is found mostly at the contact of plagioclase and clinopyroxenes (Figure 3e). Other accessory minerals are ilmenite and, rarely, apatite.



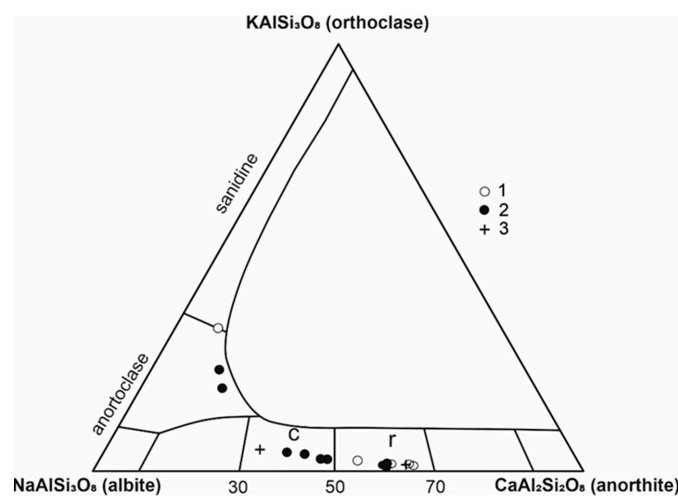


Figure 8. Classification diagram of feldspars; 1—PLKBR-2, 2—PLKOL-1; 3—gabbro cumulates, c—core, r—rims.

5. Geochemistry

The Neogene alkali basalts from Central Slovakia have a chemical composition (Table 4) similar to published analyses of basalts from similar localities [5,10,11]. In the TAS classification diagram (Figure 9), the studied basalts fall into the field of basaltic trachyan-desite (in the alkali rocks field). The alkali character of basalts and their geotectonic position is also confirmed by the contents of other trace elements. We used various discriminant diagrams for classification [37–39] (Figure 10a–c). In all used diagrams the studied basalts correspond to plate alkali basalts from the intracontinental rift. The alkaline character of the studied basalts is also documented by the REE contents, showing a significant enrichment of LREE and a decrease of the contents towards HREE (Figure 11a) and a lack of Eu anomaly. Such a pattern ($\text{La/YbN} \div 10$) suggests a lower degree of partial melting. Compared with the OIB average, the alkali basalts from Central Slovakia are slightly enriched in Rb, Ba, Th and K and slightly depleted in the remaining incompatible trace elements (Figure 11c). The analyzed alkali basalts are geochemically similar to other alkali basalts from the Panonian Basin magmatic provinces ([40–42] and others).

Table 4. Chemical composition of rocks.

Sample	PLKOL-01	PLKBR-02	Sample	PLKOL-01	PLKBR-02	Sample	PLKOL-01	PLKBR-02
SiO ₂	51.32	50.16	Sc	16.0	15.00	Y	21.00	23.80
TiO ₂	2.00	2.26	Ba	379.00	406.00	La	27.60	29.10
Al ₂ O ₃	17.19	17.60	Be	2.00	2.00	Ce	55.10	60.10
Fe ₂ O ₃ *	9.70	9.42	Co	36.70	27.90	Pr	6.47	7.22
FeO			Cs	0.80	0.90	Nd	25.40	28.10
Cr ₂ O ₃	0.01	< 0.002	Ga	18.30	19.20	Sm	5.31	5.68
MnO	0.16	0.14	Hf	4.70	5.00	Eu	1.64	1.84
CaO	7.55	7.20	Nb	37.00	40.90	Gd	5.16	5.58
MgO	5.47	4.16	Rb	47.40	49.50	Tb	0.72	0.80
Na ₂ O	4.37	4.37	Sn	2.00	3.00	Dy	4.15	4.52
K ₂ O	1.91	2.16	Sr	559.10	594.30	Ho	0.76	0.83
P ₂ O ₅	0.37	0.41	Ta	2.50	2.50	Er	1.99	2.16
LOI	0.30	1.80	Th	5.30	5.40	Tm	0.29	0.32
Total	100.35	99.68	U	1.70	1.60	Yb	1.78	1.91
			V	167.00	179.00	Lu	0.27	0.30
TOT/C	0.03	0.02	W	10.10	9.50	Ni	58.00	<20
TOT/S	<0.02	<0.02	Zr	199.90	220.50			

Fe₂O₃* total Fe as Fe₂O₃.

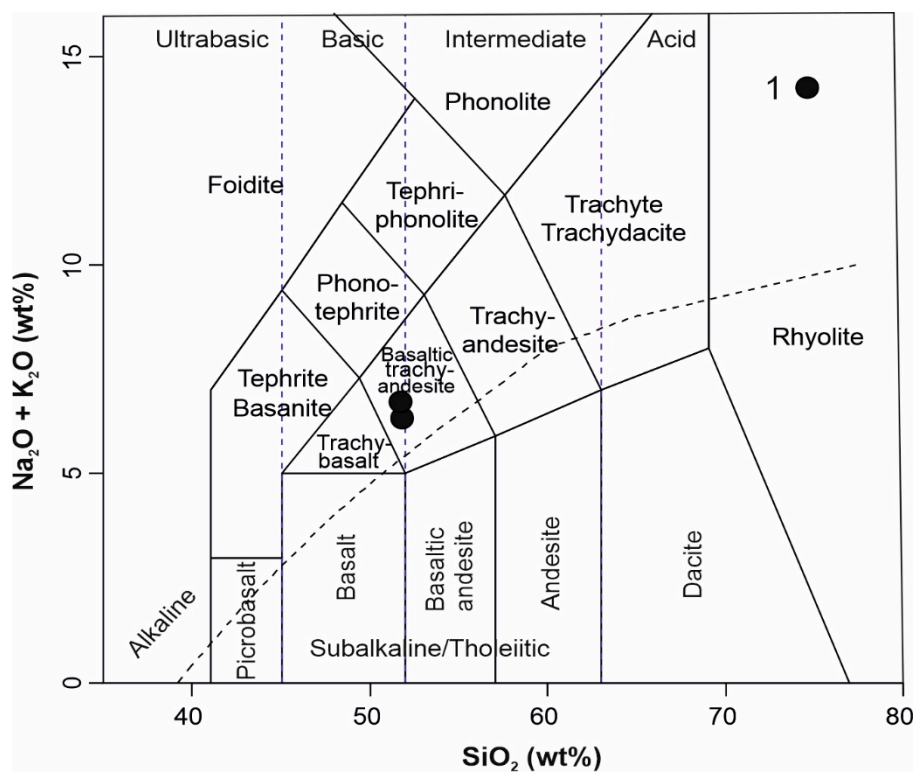


Figure 9. TAS diagram for studied basalts [43]; dashed line according to Irvin & Baragar [44], 1—studied basalts.

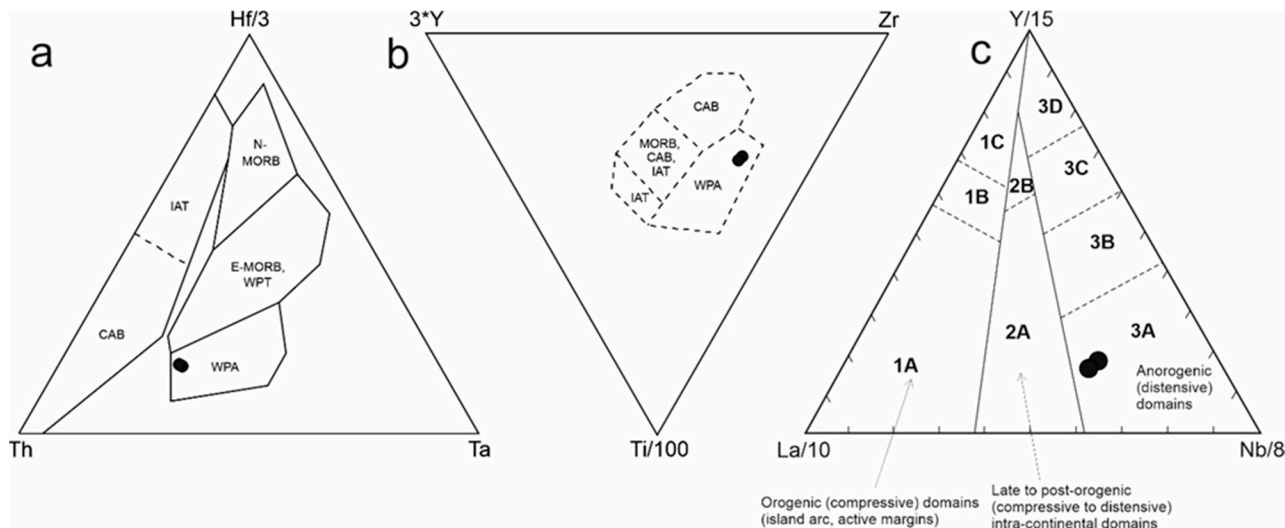


Figure 10. Discrimination diagram for basalts: (a) Th-Hf-Ta [37]; (b) Zr-Ti-Y [38]. The fields are defined as follows: N-MORB—normal Mid Ocean Ridge Basalt; E-MORB—enriched Mid Ocean Ridge Basalt; WPT—within-plate tholeiites, WPA—within-plate alkaline basalts, CAB—calc-alkaline volcanic arc basalts, IAT—island arc tholeiites. The broken lines indicate transitional zones between basalt types. (c) La-Y-Nb [39], field: 1A—CAB, 1C—volcanic arc tholeiites, 1B—overlap between 1A and 1C, 2A—continental basalts, 2B—back-arc basin basalts, 3A—WPA, 3B, 3C—E-MORB, 3D—N-MORB.

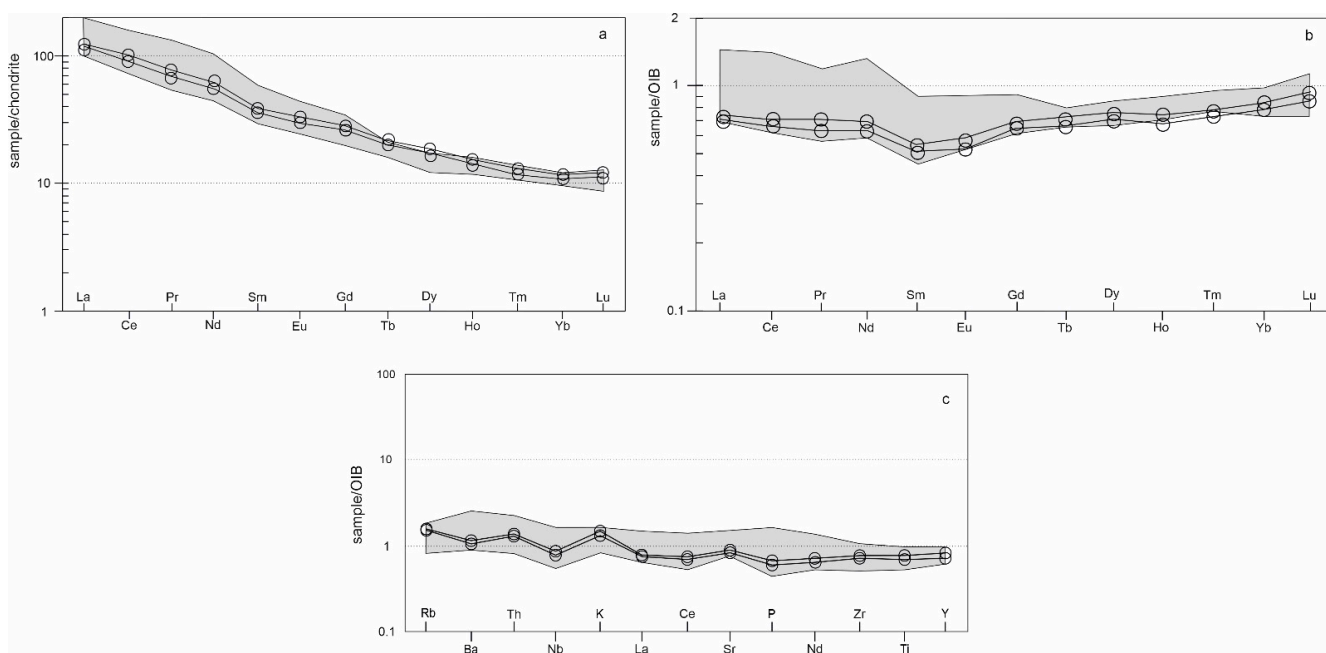


Figure 11. Spider diagrams for analyzed basalts: (a) Rare earth elements normalised to chondrite [45], (b) Rare earth elements normalised to OIB (ocean island basalt) [46], (c) incompatible trace element abundances normalised to OIB [46]. Gray fields represent analyses of Neogene alkali basalts from different Carpathian-Pannonian regions [10,11,42].

The Sr and Nd isotopic composition and radiogenic isotopes of Pb were determined in two samples (Table 5). The values of $^{143}\text{Nd}/^{144}\text{Nd}$ vs. $^{87}\text{Sr}/^{86}\text{Sr}$ isotopic ratio of the studied basalts are scattered around the value $^{143}\text{Nd}/^{144}\text{Nd}$ typical for CHUR; $^{87}\text{Sr}/^{86}\text{Sr}$ values are lower (Figure 12). Projection points of the studied basalts lie in field II, which indicates that the source material of the rocks was generated from the upper mantle. They have a higher $^{87}\text{Sr}/^{86}\text{Sr}$ isotopic ratio than MORB and HIMU. In comparison with the isotopic ratios of similar rocks, the studied basalts fall into the field of Western and Central Europe alkali basalts.

Table 5. Isotope composition of rocks.

Sample	PLKOL-01	PLKBR-02
phase	whr	whr
$^{206}\text{Pb}/^{204}\text{Pb}$	18.950458	18.944746
$\pm 2\sigma$	0.010818	0.009048
$^{207}\text{Pb}/^{204}\text{Pb}$	15.642668	15.634560
$\pm 2\sigma$	0.010757	0.009456
$^{208}\text{Pb}/^{204}\text{Pb}$	38.994356	38.962283
$\pm 2\sigma$	0.031787	0.028764
$^{207}\text{Pb}/^{206}\text{Pb}$	0.825452	0.825273
$\pm 2\sigma$	0.000174	0.000155
$^{208}\text{Pb}/^{206}\text{Pb}$	2.057709	2.056636
$\pm 2\sigma$	0.000753	0.000689
$^{87}\text{Sr}/^{86}\text{Sr}$	0.703569	0.703586
$\pm \text{abs}$	0.000004	0.000006
$^{143}\text{Nd}/^{144}\text{Nd}$	0.512779	0.512818
$\pm \text{abs}$	0.000006	0.000006
Nd	26.35	27.62
Sm	5.75	6.07

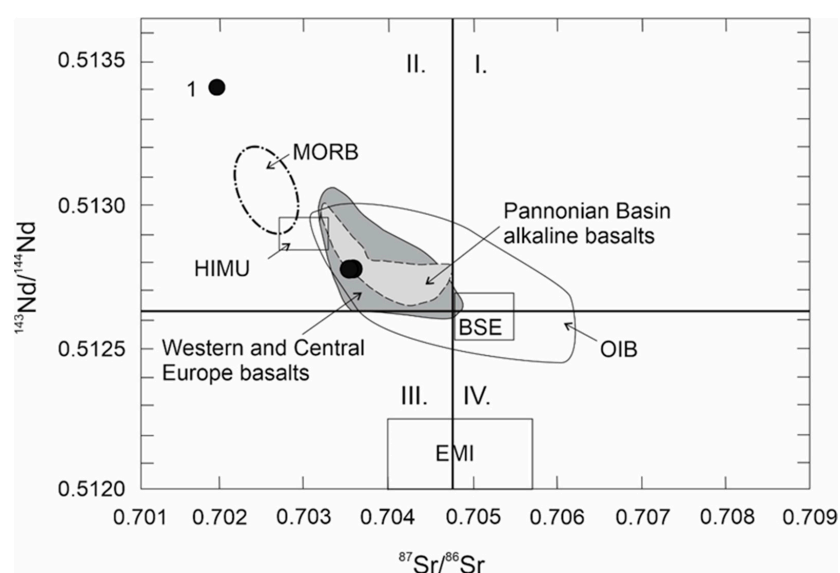


Figure 12. $^{143}\text{Nd}/^{144}\text{Nd}$ vs $^{87}\text{Sr}/^{86}\text{Sr}$ discriminant diagram. Sr and Nd isotope variations of studied alkaline basalts compared with fields of alkaline basalts from the Pannonian Basin basalts [40,47] and from alkaline basalts from Western and Central Europe [48]. HIMU (high μ refers to high $^{238}\text{U}/^{204}\text{Pb}$), BSE (Bulk Silicate Earth) according Lustrino and Wilson [49]; CHUR (chondrite uniform reservoir); OIB (oceanic island basalt) according to Faure [50], 1—studied basalts.

The diagram (Figure 13a) illustrates the isotopic ratio of $^{208}\text{Pb}/^{204}\text{Pb}$ vs. $^{206}\text{Pb}/^{204}\text{Pb}$. The studied basalts lie in the field of Pannonian Basin alkali basalts. Compared to the North Hemisphere Reference Line (NHRL), the studied basalts have a relatively lower $^{207}\text{Pb}/^{204}\text{Pb}$ ratio. The NHRL represents asthenosphere derived MORB and OIB melts. We also compared the isotope ratios $^{143}\text{Nd}/^{144}\text{Nd}$ vs. $^{206}\text{Pb}/^{204}\text{Pb}$ of the studied basalts with mantle basic derivatives (Figure 13b). The studied basalts lie outside the MORB, EAR, FOZO and HIMU fields, but they fall into the OIB field.

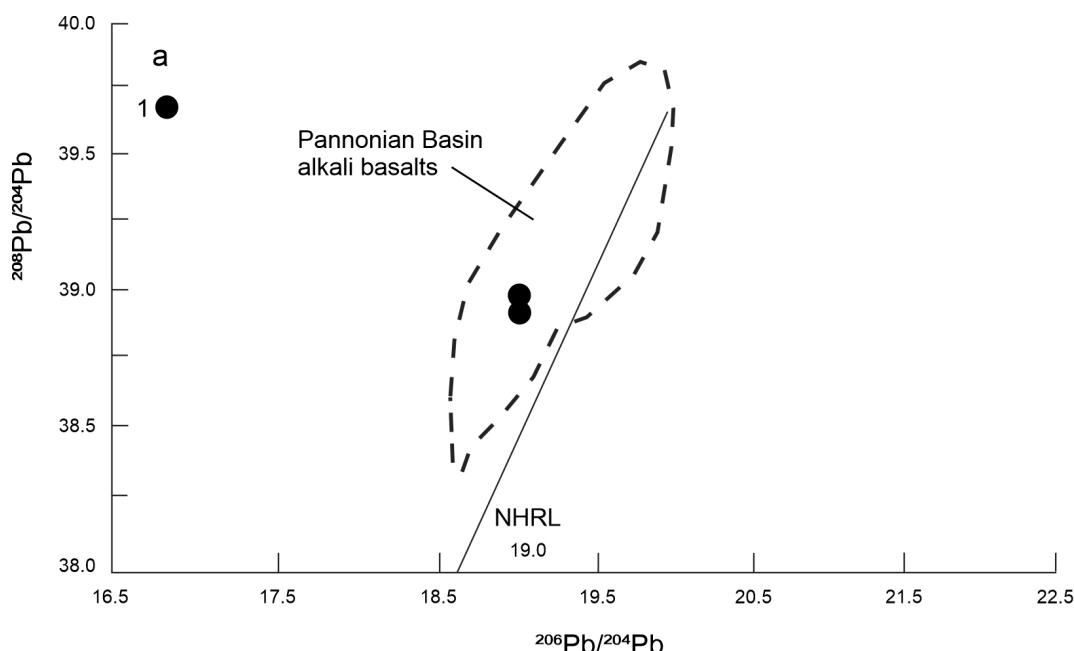


Figure 13. Cont.

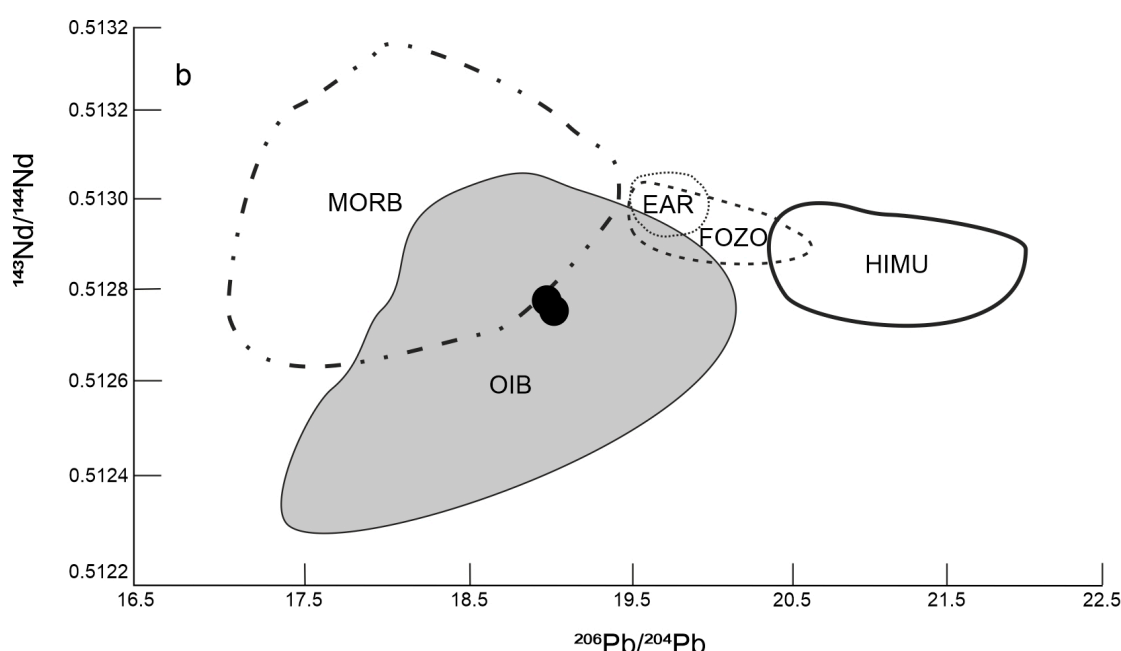


Figure 13. (a) $^{208}\text{Pb}/^{204}\text{Pb}$ vs $^{206}\text{Pb}/^{204}\text{Pb}$ discriminant diagram; dashed line—field alkali basalts from Western and Central Europe [47], NHRL from Hart [51], (b) $^{143}\text{Nd}/^{144}\text{Nd}$ vs $^{206}\text{Pb}/^{204}\text{Pb}$ diagram: mantle components (FOZO, HIMU)—from Zindler and Hart [52], EAR—from Cebriá & Wilson [53], OIB and MORB—data from Ghatak and Basu [54], Jackson and Dasgupta [55], Blasise et al. [56] and Sommer et al. [57], 1—studied basalts.

6. Discussion and Conclusions

The studied basalts are characterized by a strong zonation of Ol and Cpx. Olivines are characterized by a higher content of the forsterite component (Fo85) in the core and a lower content of the fayalite component (Fa60) in the rims. Similarly, Cpx have a significant change in the Ti/Al but also in the $\text{Al}^{\text{IV}}/\text{Al}^{\text{VI}}$ ratio (Figure 6) from core to rims. Cpx rims have higher Ti/Al ratios compared to Cpx cores, which indicates their formation at lower pressures. Based on a significant change in olivine and Cpx, we assume that basaltic magma stopped for a short time during its ascent and then the composition with Cpx rims (and also olivine rims) changed by reaction with the melt. The change in pressure (decompression) probably played a dominant role in the change of the Cpx and Ol composition. Olivines with an Fo85 and Cpx core may have been in equilibrium with primitive mantle melts and Ol and Cpx rims' compositions correspond to the equilibrium of the melt after partial crystallization of the minerals with a short stop of its movement to the surface. We used the formula of Smith et al. [58] to approximate the Cpx crystallization pressure. According to these data, Cpx cores crystallized at higher pressures (0.8 Gpa—approx. 35 km depth) than Cpx rims (0.5 Gpa—approx. 23 km depth) [59].

Various types of cumulates and xenoliths have been described from the Carpathian-Pannonian Region (CPR): spinel peridotites [60–62], pyroxenites [63,64], but also granulites [63,65] and other rock types. In the studied basalts, rare small (up to 8 mm) coarse-grained, oval-shaped cumulates are observed. They are mostly composed of Cpx and Plg. The chemical compositions of Cpx and Plg in the cumulates and the host rock are similar; therefore, we assume that these represent a sort of magma cumulates, not xenoliths.

Based on their geochemical composition, we can classify the Neogene olivine basalts from Central Slovakia as intraplate alkali basalts. This setting corresponds to their geological position—they are the result of the Late Tertiary post-orogenic extension of the Pannonian Basin following the Eocene-Miocene subduction. This is evidenced by various discrimination diagrams (Figure 10), but also by the contents of REE and other elements

(Figure 11). The contents of these elements correlate well with their contents in the compared basalts from different Carpathian-Pannonian regions [10,11,40].

Isotope compositions of Sr, Nd and Pb confirmed previous findings. From a genetic point of view, the $^{143}\text{Nd}/^{144}\text{Nd}$ and $^{87}\text{Sr}/^{86}\text{Sr}$ isotopic ratio indicate the origin of these basalts from a moderately depleted mantle source. The $^{206}\text{Pb}/^{204}\text{Pb}$ isotopic ratio has a value of about 19, which is higher than MORB but lower than HIMU. The isotope ratios are similar to OIB and to the Pannonian Basin alkali basalts.

Neogene-Quaternary mafic alkalic volcanism in the Carpathian-Pannonian region generally followed calc-alkaline volcanism. In the Central Slovakia Neogene Volcanic Field, alkalic magmas (including those in the studied area) were generated after the termination of calc-alkaline activity (8 Ma to 6.6 Ma), and a second short pulse occurred much later at ca. 0.5 Ma [66] or 0.13–0.14 Ma [67].

Central Slovakia Neogene alkalic magmatism postdated the Middle Miocene crustal thinning, which occurred mostly along the mid-Hungarian belt, where the Alcapa and Tisia-Dacia microplates were in contact since the Early Miocene. Opposite rotations of the microplates may have also contributed to crustal thinning [68]. The Central Slovakia Neogene Volcanic field including Ostrá Lúka basalts was generated by alkalic basaltic volcanism, which was accompanied by limited extensional tectonics [69]. Additional study focused on the geochemistry of alkalic rocks from other Central Slovakia Neogene Volcanic occurrences is needed to confirm these conclusions.

Author Contributions: Conceptualization, J.S. and R.P.; methodology, J.S., J.B.; resources, J.S.; R.P., data curation, J.S., J.B., V.Š.; writing—original draft preparation, J.S., R.P., J.B., V.Š., project administration, V.Š., J.S. All authors have read and agreed to the published version of the manuscript.

Funding: This research was supported by grants VEGA 1/0237/18, APVV 19-0065 and APVV-0146-16.

Data Availability Statement: Not applicable.

Acknowledgments: We thank anonymous reviewers and the editor for their constructive remarks on the manuscript. We acknowledge T. Mikuš for microprobe data acquisition.

Conflicts of Interest: We confirm that the authors have declared no conflict of interest.

References

- Wass, S.Y. Multiple origins of clinopyroxenes in alkali basaltic rocks. *Lithos* **1979**, *12*, 115–132. [[CrossRef](#)]
- Duda, A.; Schmincke, H.U. Polybaric differentiation of alkali basaltic magmas: Evidence from green-core clinopyroxenes (Eifel, FRG). *Contrib. Mineral. Petrol.* **1985**, *91*, 340–354. [[CrossRef](#)]
- Dobosi, G. Clinopyroxene zoning patterns in the young alkali basalts of Hungary and their petrogenetic significance. *Contrib. Mineral. Petrol.* **1989**, *101*, 112–121. [[CrossRef](#)]
- Dobosi, G.; Schultz-Güttler, R.; Kurat, G.; Kracher, A. Pyroxene chemistry and evolution of alkali basaltic rocks from Burgenland and Styria, Austria. *Mineral. Petrol.* **1991**, *43*, 275–292. [[CrossRef](#)]
- Dobosi, G.; Downes, H.; Matthey, D.; Embey-Isztin, A. Oxygen isotope ratios of ohenocrysts from alkali basalts of the Pannonian basin: Evidence for a O-isotopically homogenous upper mantle beneath a subduction-influenced area. *Lithos* **1998**, *42*, 213–223. [[CrossRef](#)]
- Fodor, R.V.; Dobosi, G.; Sial, A.N. Zoned clinopyroxenes in alkali basalt: Clues to fractionation and magma-mixing histories for seemingly primitive magmas. *Chem. Der Erde* **1995**, *55*, 133–148.
- Embey-Isztin, A.; Dobosi, G. Composition of olivines in the young alkali basalts and their peridotite xenoliths from the Pannonian basin. *Ann. Hist. Nat. Musei Natl. Hung.* **2007**, *99*, 5–22.
- Jankovics, M.E.; Dobosi, G.; Embey-Isztin, A.; Kiss, B.; Sági, T.; Harangi, S.; Ntaflos, T. Origin and ascent history of unusually crystal-rich alkalic basaltic magmas from the western Pannonian basin. *Bull. Volcanol.* **2013**, *75*, 749. [[CrossRef](#)]
- Jankovics, M.E.; Taracsák, Z.; Dobosi, G.; Embey-Isztin, A.; Batki, A.; Harangi, S.; Hauzenberger, C.A. Clinopyroxene with diverse origin in alkalic basalts from western Pannonian Basin: Implications from trace elements characteristics. *Lithos* **2016**, *262*, 120–134. [[CrossRef](#)]
- Mihaliková, A.; Šimová, M. Geochémia a petrologia miocénno-pleistocénnych alkalickej bazaltov stredného Slovenska. *Západné Karp. Sérija Miner. Petrogr. Geochémia Met.* **1989**, *12*, 7–142.
- Harangi, S.; Lenkey, L. Genesis of the Neogene to Quaternary volcanism in the Carpathian-Pannonian region: Role of subduction, extension and mantle plume. *Geol. Soc. Am. Spec. Pap.* **2007**, *418*, 67–92. [[CrossRef](#)]
- Kantor, J.; Wiegerová, V. Radiometrics ages of some basalts of Slovakia by K/Ar method. *Geol. Carpathica* **1981**, *32*, 29–34.

13. Lexa, J.; Konečný, V.; Kaličiak, M.; Hojstričová, V. Space –time distribution of volcanics in the Carpatho-Panonian region. In *Geodynamic Model and Deep Structure of the Western Carpathians*; Rakús, M., Vozár, J., Eds.; GUDŠ: Bratislava, Slovakia, 1993; pp. 57–70. (In Slovak)
14. Konečný, V.; Lexa, J.; Balogh, K.; Konečný, P. Alkali basalt volcanism in Southern Slovakia: Volcanic forms and time evolution. *Acta Vulcanol.* **1995**, *7*, 167–171.
15. Konečný, V.; Lexa, J.; Balogh, K. Neogene-Quaternary alkali basalt volcanism of Slovakia: Review of volcanic forms and evolution. *Geol. Carpathica Spec. Issue* **1999**, *50*, 112–115.
16. Konečný, V.; Balogh, K.; Orlický, O.; Vass, D.; Lexa, J. Timing of the Neogene-Quaternary alkali basalt volcanism in Central and Southern Slovakia (Western Carpathians). In Proceedings of the XVII Congress of Carpathian-Balkan Geological Association, Bratislava, Slovakia, 1–4 September 2002; p. 53.
17. Kaličiak, M.; Žec, B. Review of Neogene volcanism of Eastern Slovakia. *Acta Vulcanol. Spec. Issue* **1995**, *7*, 87–95.
18. Vass, D.; Began, A.; Gross, P.; Kahan, Š.; Krystek, I.; Kohler, E.; Lexa, J.; Nemčok, J.; Ružička, M.; Vaškovský, I. *The Regional Geological Division of the Western Carpathians and Northern Part of the Pannonian Basin*, 1:500000; Dionýz Štúr Publishers: Bratislava, Slovakia, 1988.
19. Harangi, S.; Jankovics, M.É.; Sági, T.; Kiss, B.; Lukács, R.; Soós, I. Origin and geodynamic relationships of the Late Miocene to Quaternary alkaline basalt volcanism in the Pannonian basin, eastern-central Europe. *Int. J. Earth Sci.* **2015**, *104*, 2007–2032. [[CrossRef](#)]
20. Chernyshev, I.V.; Konečný, V.; Lexa, J.; Kovalenker, V.A.; Jeleň, S.; Lebedev, V.A.; Goltsman, Y.V. K-Ar and Rb-Sr geochronology and evolution of the Štiavnicka Stratovolcano (Central Slovakia). *Geol. Carpathica* **2013**, *64*, 327–351. [[CrossRef](#)]
21. Lexa, J.; Seghedi, I.; Németh, K.; Szakács, A.; Konečný, V.; Pécsay, Z.; Fülöp, A.; Kovacs, M. Neogene-Quaternary Volcanic forms in the Carpathian-Pannonic Region: A review. *Cent. Eur. J. Geosci.* **2010**, *2*, 207–270. [[CrossRef](#)]
22. Konečný, V.; Bezák, V.; Halouzka, R.; Stolár, M.; Dublan, L. *Geological Map of Javorie 1:50 000*; Geol. Surv. SR: Bratislava, Slovakia, 1998.
23. Konečný, V.; Lexa, J.; Halouzka, R.; Dublan, L.; Šimon, L.; Stolár, M.; Nagy, A.; Polák, M.; Vozár, J.; Havrla, M.; et al. *Geological Map of Štiavnické Vrchy Mts. And Pohronský Inovec Mts*; Geol. Surv. SR: Bratislava, Slovakia, 1998.
24. Lexa, J.; Konečný, V. Geodynamic aspects of the Neogene to Quaternary volcanism. In *Geodynamic Development of the Western Carpathians*; Rakús, M., Ed.; Geologická služba SR: Bratislava, Slovakia, 1998; pp. 219–240.
25. Konečný, V.; Lexa, J.; Planderová, E. Stratigraphy of the Central Slovakia Neogene Volcanic Field. *Západ. Karp. Sér. Geol.* **1983**, *9*, 1–203. (In Slovak with English summary)
26. Konečný, V.; Bezák, V.; Halouzka, R.; Konečný, O.; Miháliková, A.; Marcin, D.; Iglárová, L.; Panáček, A.; Štohl, J.; Žáková, E.; et al. *Explanatory Notes to the Geological Map of Javorie*; Geol. Surv. SR: Bratislava, Slovakia, 1998; pp. 1–304. (In Slovak with English summary)
27. Konečný, V.; Lexa, J.; Halouzka, R.; Hók, J.; Vozár, J.; Dublan, L.; Nagy, A.; Šimon, L.; Havrla, M.; Ivanička, J.; et al. *Explanatory Notes to the Geological Map of Štiavnické Vrchy and Pohronský Inovec Mountain Ranges (Štiavnicka Stratovolcano)*; Geol. Surv. SR: Bratislava, Slovakia, 1998; pp. 1–473. (In Slovak with English summary)
28. Horwitz, E.P.; Chiarizia, R.; Dietz, M.L. A novel strontium-selective extraction chromatographic resin. *Solvent Extr. Ion Exch.* **1992**, *10*, 313–336. [[CrossRef](#)]
29. Todt, W.; Cliff, R.A.; Hanser, A.; Hofmann, A.W. Re-calibration of NBS lead standards using 202Pb + 205Pb double spike. *Terra Abstr.* **1993**, *5*, 396.
30. Ali, S.; Ntaflos, T. Alkali basalts from Burgenland, Austria: Petrological constraints on the origin of the westernmost magmatism in the Carpathian-Pannonic Region. *Lithos* **2011**, *121*, 176–188. [[CrossRef](#)]
31. Thomson, A.; MacLennan, J. The distribution of olivine composition in Icelandic basalts and picrites. *J. Petrol.* **2013**, *54*, 745–768. [[CrossRef](#)]
32. Goff, F.E. Vesicle cylinders in vapor-differentiated basalt flows. *J. Volcanol. Geotherm. Res.* **1996**, *71*, 167–185. [[CrossRef](#)]
33. Clément, J.P.; Caroff, M.; Dudoignon, P.; Launeau, P.; Bohn, M.; Cotton, J.; Blais, S.; Guille, G. A possible link between gabbros bearing High Temperature Iddingsite alteration and huge pegmatoid intrusions: The Society Islands, French Polynesia. *Lithos* **2007**, *96*, 524–542. [[CrossRef](#)]
34. Tschepp, C.; Ntaflos, T.; Kiraly, F.; Harangi, S. High temperature corrosion of olivine phenocrysts in Pliocene basalts from Banat, Romania. *Aust. J. Earth Sci.* **2010**, *103*, 101–110.
35. Morimoto, N.; Fabries, J.; Ferguson, A.K.; Ginzburg, I.V.; Ross, M.; Seifert, F.A.; Zussman, J.; Aoki, K.; Gottardi, G. Nomenclature of pyroxenes. *Amer. Mineral.* **1988**, *73*, 1123–1133.
36. Aoki, K.; Kushiro, I. Some clinopyroxenes from ultramafic inclusions in Dreiser Weiher, Eifel. *Contrib. Mineral. Petrol.* **1968**, *18*, 326–337. [[CrossRef](#)]
37. Wood, D.A. The application of a Th-Hf-Ta diagram to problems of tectonomagmatic classification and to establishing the nature of crustal contamination of basaltic lavas of the British Tertiary volcanic province. *Earth Planet. Sci. Lett.* **1980**, *50*, 11–30. [[CrossRef](#)]
38. Pearce, J.A.; Cann, J. Tectonic setting of basic volcanic rocks determined using trace element analysis. *Earth Planet. Sci. Lett.* **1973**, *19*, 290–300. [[CrossRef](#)]
39. Cabanis, B.; Lecolle, M. Le diagramme La/10-Y/15-Nb/8: Un outil pour la discrimination des séries volcaniques et la mise en évidence des processus de mélange et/ou de contamination crustale. *C. R. Acad. Sci.* **1989**, *2*, 2023–2029.

40. Embey-Isztin, A.; Downes, H.; James, D.E.; Upton, B.G.J.; Dobosi, G.; Ingram, G.A.; Harmon, R.S.; Scharbert, H.G. The petrogenesis of Pliocene alkaline volcanic rocks from the Pannonian Basin, Eastern Central Europe. *J. Petrol.* **1993**, *34*, 317–343. [[CrossRef](#)]
41. Embey-Isztin, A.; Dobosi, G.; James, D.; Downer, H.; Poultidis, C.; Scharbert, H. A compilation of new major, trace element and isotope geochemical analyses of the young alkali basalts from the Pannonian Basin. *Fragm. Mineral. Palaeo.* **1993**, *16*, 5–26.
42. Downes, H.; Seghedi, I.; Szakács, A.; Dobosi, G.; James, D.E.; Vaselli, O.; Rigby, I.J.; Ingram, G.A.; Rex, D.; Pécsay, Z. Petrology and geochemistry of late Tertiary/Quaternary mafic alkaline volcanism in Romania. *Lithos* **1995**, *35*, 65–81. [[CrossRef](#)]
43. Le Maitre, R.W.; Bateman, P.; Dudek, A.; Keller, J.; Lameyre, J.; Le Bas, M.J.; Sabine, P.A.; Schmid, R.; Sørensen, H.; Streckeisen, A.; et al. *A Classification of Igneous Rocks and Glossary of Terms. Recommendations of the International Union of Geological Sciences. Subcommission on the Systematics of Igneous Rocks*; Blackwell Scientific Publications: Cambridge, UK, 1989; p. 193.
44. Irvin, T.N.; Baragar, W.R.A. A guide to the chemical classification of the common volcanic rocks. *Can. J. Earth Sci.* **1971**, *8*, 523–548. [[CrossRef](#)]
45. McDonough, W.F.; Sun, S.S. The composition of the Earth. *Chem. Geol.* **1995**, *120*, 223–253. [[CrossRef](#)]
46. McDonough, W.F.; Sun, S.S.; Ringwood, A.E.; Jagoutz, E.; Hofmann, A.W. Potassium, rubidium and cesium in the Earth and Moon and the evolution of the Earth. *Geochim. Cosmochim. Acta* **1992**, *56*, 1001–1012. [[CrossRef](#)]
47. Salters, V.J.M.; Hart, S.R.; Pantó, G. Origin of late Cenozoic volcanic rocks of the Carpathian Arc, Hungary. In *The Pannonian Basin: A Study in Basin Evolution*; Royden, L.H., Horvath, F., Eds.; American Association of Petroleum Geologists: Tulsa, OK, USA, 1988; Volume 45, pp. 279–292. [[CrossRef](#)]
48. Wilson, M.; Downes, H. Tertiary-Quaternary extension-related alkaline magmatism in Western and Central Europe. *J. Petrol.* **1991**, *32*, 811–849. [[CrossRef](#)]
49. Lustrino, M.; Wilson, M. The circum-Mediterranean anorogenic Cenozoic igneous province. *Earth Sci. Rev.* **2007**, *81*, 1–65. [[CrossRef](#)]
50. Faure, G. *Principles of Isotope Geology*; John Wiley and Sons: New York, NY, USA, 1986; p. 589.
51. Hart, S.R. A large isotope anomaly in the Southern Hemisphere mantle. *Nature* **1984**, *309*, 753–757. [[CrossRef](#)]
52. Zindler, A.; Hart, S. Chemical geodynamics. *Ann. Rev. Earth Planet. Sci.* **1986**, *14*, 493–571. [[CrossRef](#)]
53. Cebriá, J.M.; Wilson, M. Cenozoic mafic magmatism in Western/Central Europe: A common European asthenospheric reservoir. *Terra Nova Abstr. Suppl.* **1995**, *7*, 162.
54. Ghatak, A.; Basu, A.R. Vestiges of the Kerguelen plume in the Sylhet Traps, northeastern India. *Earth Planet. Sci. Lett.* **2011**, *308*, 52–64. [[CrossRef](#)]
55. Jackson, M.G.; Dasgupta, R. Compositions of HIMU, EM1, and EM2 from global trends between radiogenic isotopes and major elements in ocean island basalts. *Earth Planet. Sci. Lett.* **2008**, *276*, 175–186. [[CrossRef](#)]
56. Blaise, N.; Ngongang, T.; Kamgang, P.; Chazot, G.; Agranier, A.; Bellon, H.; Nonnotte, P. Age, geochemical characteristics and petrogenesis of Cenozoic intraplate alkaline volcanic rocks in the Bafang region, West Cameroon. *J. Afr. Earth Sci.* **2015**, *102*, 218–232. [[CrossRef](#)]
57. Sommer, C.A.; Barreto, C.J.S.; Lafon, J.M.; De Lima, E.F.; Alexandre, F.M.; Chemale, F., Jr.; Koester, E. Pb isotope geochemistry and reappraisal of Sr-Nd isotopes of the Cerro Morado basic magmatism (Ischigualasto-Villa Union Triassic basin, NW Argentina): Implications for the mantle sources. *Braz. J. Geol.* **2018**, *48*, 115–126. [[CrossRef](#)]
58. Smith, I.E.M.; Vavassis, I.; De Bono, A.; Rosselet, F.; Matti, B.; Bellini, M. Deep-seated fractional during the rise of small-volume basalt magma batch: Crater Hill, ASuckland, New Zealand. *Contrib. Mineral. Petrol.* **2008**, *155*, 511–527. [[CrossRef](#)]
59. Lee, C.T.; Luffi, P.; Plank, T.; Dalton, H.; Leeman, W.P. Constraints on the depths and temperatures of basaltic magma generation on Earth and other terrestrial planets using new thermobarometers for mafic magmas. *Earth Planet. Sci. Lett.* **2009**, *279*, 20–33. [[CrossRef](#)]
60. Downes, H.; Embey-Isztin, A.; Thirlwall, M.F. Petrology and geochemistry of spinel peridotite xenoliths from the western Pannonian Basin (Hungary): Evidence for an association between enrichment and texture in the upper mantle. *Contrib. Mineral. Petrol.* **1992**, *109*, 340–354. [[CrossRef](#)]
61. Hovorka, D.; Fejdi, P. Spinell peridotite xenoliths in the West Carpathian Late Cenozoic alkali basalts and their tectonic significance. *Bull. Volcanol.* **1980**, *43*, 95–106. [[CrossRef](#)]
62. Szabo, C.; Falus, G.; Zajacz, Z.; Kovács, I.; Bali, E. Composition and evolution of lithosphere beneath the Carpathian–Pannonian Region: A review. *Tectonophysics* **2004**, *393*, 119–137. [[CrossRef](#)]
63. Kempton, P.D.; Downes, H.; Embey-Isztin, A. Mafic granulite xenoliths in Neogene alkali basalts from the Western Pannonian Basin: Insights into the lower crust of a collapsed orogen. *J. Petrol.* **1997**, *38*, 941–970. [[CrossRef](#)]
64. Dobosi, G.; Downes, H.; Embey-Isztin, A.; Jenner, G.A. Origin of megacrysts and pyroxenite xenoliths from the Pliocene alkali basalts of the Pannonian Basin (Hungary). *N. Jb. Mineral. Abh.* **2003**, *178*, 217–237. [[CrossRef](#)]
65. Dobosi, G.; Kempton, P.; Downes, H.; Embey-Isztin, A.; Thirlwall, M.; Greenwood, P. Lower crustal granulite xenoliths from the Pannonian Basin, Hungary, Part 2: Sr-Nd-Pb-Hf and O isotope evidence for formation of continental lower crust by tectonic emplacement of oceanic crust. *Contrib. Mineral. Petrol.* **2003**, *144*, 671–683. [[CrossRef](#)]
66. Balogh, K.; Mihálková, A.; Vass, D. Radiometric dating of basalts in southern and central Slovakia. *Záp. Karp. Ser. Geol.* **1981**, *7*, 113–126.

67. Šimon, L.; Halouzka, R. Pútikov vršok volcano: The youngest volcano in the Western Carpathians. *Slovak Geol. Mag.* **1996**, *2*, 103–123.
68. Csontos, L.; Nagymarosy, A. The Mid-Hungarian line: A zone of repeated tectonic inversions. *Tectonophysics* **1998**, *297*, 51–71. [[CrossRef](#)]
69. Fodor, L.; Csontos, L.; Bada, G.; Györfi, I.; Benkovics, L. Cenozoic tectonic evolution of the Pannonian basin system and neighbouring orogens: A new synthesis of paleostress data. In *The Mediterranean Basins: Cenozoic Extension within the Alpine Orogeny*; Durand, B., Jolivet, L., Horváth, F., Séranne, M., Eds.; Geol. Soc. London, Spec. Publ.: London, UK, 1999; Volume 156, pp. 295–334.